Construction and Building Materials 337 (2022) 127613

Contents lists available at ScienceDirect

Construction and Building Materials

journal homepage: www.elsevier.com/locate/conbuildmat

Innovative modeling framework of chloride resistance of recycled aggregate concrete using ensemble-machine-learning methods

Kai-Hua Liu [a], Jia-Kai Zheng [a], Fernando Pacheco-Torgal [b], Xin-Yu Zhao [c,*]

[a] School of Civil and Transportation Engineering, Guangdong University of Technology, Guangzhou 510006, China
[b] University of Minho, C-TAC Research Centre, Engineering School, Guimarães, Portugal
[c] State Key Laboratory of Subtropical Building Science, South China University of Technology, Guangzhou 510641, China

ARTICLE INFO

Keywords:
Recycled aggregate concrete
Chloride penetration
Machine learning
Model interpretability
Mixture
Service life prediction

ABSTRACT

This study investigates the feasibility of introducing machine learning algorithms to predict the diffusion resistance to chloride penetration of recycled aggregate concrete (RAC). A total of 226 samples collated from published literature were used to train and test the developed machine learning framework, which integrated four standalone models and two ensemble models. The hyperparameters involved were fine-tuned by grid search and 10-fold cross-validation. Results showed that all the models had good performance in predicting the chloride penetration resistance of RAC and among them, the gradient boosting model outperformed the others. The water content was identified as the most critical factor affecting the chloride ion permeability of RAC based on the standardized regression coefficient analysis. The model's interpretability was greatly improved through a two-way partial dependence analysis. Finally, based on the proposed machine learning models, a performance-based mixture design method and a service life prediction approach for RAC were developed, thereby offering novel and robust design tools for achieving more durable and resilient development goals in procuring sustainable concrete.

1. Introduction

Sand and gravel are the largest portion of resource materials used in the built environment and the most extracted materials around the world [1]. At the same time, the amount of construction and demolition wastes (CDW) is growing rapidly with the acceleration of urbanization process worldwide [2]. This makes the circular economy crucial for sustainable development and the valorization of CDW of paramount importance for the construction industry [3,4]. With these predicaments, the reuse of CDW becomes inevitable.

Concrete recycling, among many other strategies in support of sustainability, is technically feasible. Waste valorization is achieved by crushing concrete rubble into recycled aggregates (RA) and then being used to replace, partly or totally, natural aggregate (NA) in new concrete manufacture [5]. Despite some negative effects brought by such substitution, the resulting products, i.e., recycled aggregate concrete (RAC), is believed to be able to meet general engineering needs [6–9]. As a result, RAC is increasingly encouraged for structural applications [10–12].

Chloride ion ingress will cause corrosion of steel reinforcement in concrete and, hence, reduce safety and durability of structures [13]. Understanding the resistance to chloride erosion of RAC is a prerequisite for ensuring its durability robustness and boosting its use. Generally, RAC is marked to be less resistant to chloride penetration than its natural aggregate concrete (NAC) counterpart [14,15]. This happens because the porous structure of adhered mortar to RA renders RAC more permeable and, in technical terms, elevates its chloride penetration rate and chloride migration coefficient [16]. As RA replacement ratio increases, the chloride resistance of RAC decreases [17,18], especially for cases where fine RA is incorporated [19]. Reducing the water-cement ratio [20], prolonging curing time [21], and adding mineral admixtures (fly ash [22], silica fume [23], blast furnace slag [24], etc.) can

Abbreviations: NA, natural aggregates; RA, recycled aggregates; RAC, recycled aggregate concrete; NAC, natural aggregate concrete; ML, machine learning; ANN, artificial neural network; GPR, Gaussian process regression; SVR, support vector regression; CART, classification and regression tree; RF, random forest; GBDT, gradient boosting decision trees; CEF, coulomb passed electric charge; RCM, rapid chloride ions migration coefficient; RMSE, root mean square error; SI, scattering index; MAPE, mean absolute percentage error; VIF, variance inflation factor; SRC, standardized regression coefficient; CSH, calcium silicate hydrate.

* Corresponding author.
E-mail address: ctzhaoxy@scut.edu.cn (X.-Y. Zhao).

https://doi.org/10.1016/j.conbuildmat.2022.127613
Received 26 December 2021; Received in revised form 14 March 2022; Accepted 20 April 2022

compensate for the side effects of RA and in turn enhance the resistance of RAC to chloride-induced deterioration. Due to the high uncertainty of RA, some authors suggested that there is no significant difference in the chloride diffusion between NAC and RAC [25,26]. Yet in other cases, the chloride resistance of RAC is reported to be even slightly higher than that of NAC [27]. On the plus side, the porosity of RA could provide an internal curing effect [28] and additional chloride binding capacity for RAC [29], which is conducive to improved chloride resistance. But these beneficial effects are hard to quantify and likely to be offset by the negative contributions. Taken together, the foregoing studies indicate that the impact of RA incorporation on the chloride penetration of RAC is complex; the issue remains controversial, and different approaches to address it are sorely needed.

Experiment method is regarded as the most direct way to investigate RAC's durability performance; however, it is time-consuming and costly. On the other hand, numerical and analytical methods are helpful, but still difficult to replicate the characteristics of RAC. Notably, in recent years artificial intelligence (AI) has developed rapidly, which is changing the way humans perceive the world [30]. As a subset of AI, machine learning (ML) has become a key enabling technology in multiple regimes of civil engineering [31]. Compared with traditional methods, ML can achieve more desirable results at a lower cost [32,33]. Several researchers have tried to introduce ML methods into the evaluation of RAC's attributes. Topçu and Sarıdemir [34] showed that the artificial neural network (ANN) and fuzzy logic (FL) have good potential in predicting the mechanical performance of RAC. Omran et al. [35] compared different ML algorithms on estimating the compressive strength of RAC and found all models can obtain good results with their coefficients of determination higher than 0.90. It was confirmed by Duan et al. [36] that ANN can be leveraged to predict the compressive strength and elastic modulus of RAC with high accuracy—so can it determine the classification of RA. Similar results were observed by Golafshani et al. [37] and Naderpour et al. [38]. Xu et al. [39] performed a sensitivity analysis on the parameters affecting the triaxial behavior of RAC using grey correlation; several ML algorithms were then developed which showed superior accuracy over empirical models. Note that existing ML-based studies focus mainly on forecasting the mechanical properties of RAC, while research on predicting the durability of RAC is scarce. An attempt is thus worthwhile in this regard, as recent studies [40,41] have shown the utility of ML methods for evaluating the durability of concrete.

Chloride attack on concrete is a sophisticated process that is affected by many factors. The meso-pores as well as micro-pores present in RA [42] and the existence of multiple interfacial transition zones [43] further complicate this process. Unlike traditional methods, ML algorithms provide an unprecedented pattern that allows identifying the hidden and interrelated mechanisms behind a complex system by data mining. This paper presents a novel modeling framework for predicting the chloride penetration resistance of RAC. The framework integrated a host of ML methods, including four standalone methods (artificial neural network, Gaussian process regression, support vector regression, and decision tree) and two ensemble methods (random forest and gradient boosting). With the dataset collated from published literature, the incorporated ML models were developed, discussed, and compared. The importance of each input variable was revealed through standardized regression coefficient analysis. Moreover, calculations drawing on the partial dependence concept were made to improve the models' interpretability. Finally, a performance-based mixture design method and a service life prediction approach were proposed for RAC structures based on the validated models.

2. Methodology

In this section, the principles of each ML algorithm included in the framework are briefly described, which helps understand the key ideas as well as compare their differences.

2.1. Artificial neural network (ANN)

ANN is perhaps the most popular ML model yet. It mimics the human nervous system to establish input–output relationships [44]. The first layer of an ANN model is the input layer, the last is the output layer, and what connects the two is the hidden layer(s). Each layer has neurons that receive input signals and generate outputs through a transfer function. Each connection is assigned a weight, which modifies the strength of signals sent downstream. In addition to weights, there is another crucial parameter called bias. Weights and biases are initially assigned random values and then adjusted to reduce the errors between the predicted and observed values.

2.2. Gaussian process regression (GPR)

GPR is a non-parametric regression method, which is based on Bayesian theory. It continuously updates the posterior probability distribution through measured data until the posterior distribution basically matches the real distribution. Compared with other ML algorithms, GPR is more of a kernel-based algorithm designed for small samples and has advantages in solving problems with a high degree of nonlinearity [45]. It quantifies the uncertainty of predictions in a principled way.

2.3. Support vector regression (SVR)

In a broader scope, the support vector machine (SVM) is an algorithm based on statistical learning, developed from optimal hyperplane with linear differentiability [46]. When SVM is extended for regression analysis, it becomes SVR. The advantage of SVR lies in that it can approximate complex nonlinear continuous functions with high accuracy, especially be suitable for the small sample size.

2.4. Classification and regression tree (CART)

The Decision tree (DT) has an inverted tree-like structure consisting of nodes and directed edges. Each node in the tree represents a test for a certain feature, while each branch corresponds to a result of the test for that feature. The Classification and regression tree (CART) model is a widely used DT method, among its many variants [47]. It is composed of feature selection, tree generation, and pruning. As a powerful tool for classification and regression, CART uses a heuristic method to divide the input space. It traverses all input variables to find the optimal segmentation variable, recursively divides each region into two sub-regions, and determines the output value on each sub-region.

2.5. Random forest (RF)

Bagging is an ensemble ML algorithm that draws datasets from original data with put-back to train the model. RF is a type of bagging, which adopts decision trees as weak learners [47]. By aggregating multiple decision trees and improving the prediction accuracy through voting or averaging, the RF model has high accuracy and better generalization ability. For a regression problem, the prediction of RF $K(x)$ can be calculated as:

$$K(x) = \frac{1}{T}\sum_{i=1}^{T} k_i(x) \tag{1}$$

where $k_i(x)$ is the predicted value of i^{th} decision tree; and T represents the number of trees.

2.6. Gradient boosting decision trees (GBDT)

Boosting is another ensemble ML algorithm. It is composed of a series of dependent base learners with different weights. Gradient boosting (GB) belongs to the category of boosting. It borrows the idea of gradient

descent, trains the newly added weak learner according to the negative gradient information of the current model loss function, and combines the trained weak learner into the current model in an accumulated form [48]. GB using decision trees as weak learners is GBDT. This algorithm can be formulated as:

$$G_0 = \underset{\lambda}{\operatorname{argmin}} \sum_{i=1}^{T} L(y_i, \lambda) \tag{2}$$

$$G_r = G_{r-1} + \underset{h_r \in H}{\operatorname{argmin}} \sum_{i=1}^{T} [L(y_i, G_{r-1}(x_i) + h_r(x_i))] \tag{3}$$

$$\nabla Loss = \frac{\partial L(y_i, G_{r-1}(x_i))}{\partial G_{r-1}(x_i)} \tag{4}$$

where G_0 represents the initial weak learner, G_r represents the final strong learner, h_r represents the subsequent weak learner, $\nabla Loss$ represents the gradient for the loss function.

3. Dataset description

There are two common methods to evaluate the chloride penetration resistance of concrete, i.e., the Coulomb passed electric charge (CEF) method and the rapid chloride ions migration coefficient (RCM) method [49]. The CEF method evaluates chloride penetration of concrete by measuring the electric charge passed through specimens at a specified voltage and energization time. It has the advantages of easy operation, short test period, and high stability of test results, which make it one of the most accepted methods for evaluation of chloride resistance of concrete. By comparison, the RCM method measures the chloride ion diffusion coefficient of concrete according to Fick's second law. Although this method enables an expeditious quantitative calculation of chloride penetration, it is more complicated and less convenient than the CEF method. In addition, based on a thorough review of existing studies, there are relatively few test results using the RCM method. Therefore, only test data from the CEF method were used to quantify the chloride durability of RAC.

The factors affecting the chloride penetration of RAC were grouped into three categories. The first is related to the RAC mixture, including the amounts of cement (**C**), water (**W**), sand (**S**), natural coarse aggregate (**NCA**), recycled coarse aggregate (**RCA**), and mineral admixtures (fly ash (**FA**) and ground granulated blast slag (**GGBS**)). The second is related to aggregates quality, including the water absorption (**WA**) and the apparent density (**D**) of aggregates. Considering the NCA and RCA were mixed to prepare the RAC, the WA and D of the mixed aggregates were calculated by a weighted method as follows [37]:

$$\mathrm{WA} = \mathrm{WA_{RCA}} \times m_{\mathrm{RCA}}/(m_{\mathrm{NCA}} + m_{\mathrm{RCA}}) + \mathrm{WA_{NCA}} \times m_{\mathrm{NCA}}/(m_{\mathrm{NCA}} + m_{\mathrm{RCA}}) \tag{5}$$

$$\mathrm{D} = \mathrm{D_{RCA}} \times m_{\mathrm{RCA}}/(m_{\mathrm{NCA}} + m_{\mathrm{RCA}}) + \mathrm{D_{NCA}} \times m_{\mathrm{NCA}}/(m_{\mathrm{NCA}} + m_{\mathrm{RCA}}) \tag{6}$$

where $\mathrm{WA_{RCA}}$ and $\mathrm{WA_{NCA}}$ represent the water absorption of RCA and NCA, respectively; m_{RCA} and m_{NCA} represent the amounts of RCA and NCA, respectively; $\mathrm{D_{RCA}}$ and $\mathrm{D_{NCA}}$ are the apparent density of RCA and NCA, respectively. The third factor is concrete curing. Only one factor, i.e., the curing age (**CA**), was considered. Finally, an experimental database including 226 samples related to the chloride penetration resistance of RAC from the available literature [50–60] was established (Table A1), in which the three groups of parameters (as input variables) were well defined and documented.

4. Performance measurements

To quantitatively evaluate the prediction performance of each ML method in the framework, four statistical parameters were used, including root mean square error (RMSE), scattering index (SI), mean absolute percentage error (MAPE), and determination of coefficient (R^2):

$$\mathrm{RMSE} = \sqrt{\sum_{i=1}^{m} (e_i - p_i)^2/m} \tag{7}$$

$$\mathrm{SI} = \mathrm{RMSE}/\overline{e}_i \tag{8}$$

$$\mathrm{MAPE} = 100\% \left(\sum_{i=1}^{m} |(e_i - p_i)/e_i| \right) \Big/ m \tag{9}$$

$$\mathrm{R^2} = \left[\frac{\sum_{i=1}^{m} (e_i - \overline{e}_i)(p_i - \overline{p}_i)}{\sqrt{\sum_{i=1}^{m} (e_i - \overline{e}_i)^2 \sum_{i=1}^{m} (p_i - \overline{p}_i)^2}} \right]^2 \tag{10}$$

where m represents the number of samples; e_i and p_i represent the experimental and predicted results, respectively; $\overline{e}_i$ and $\overline{p}_i$ represent the average of e_i and p_i values, respectively. A good model should have a higher R^2 and lower RMSE, SI, and MAPE.

In some cases, different performance measures may probably give different estimates. To avoid this trap, a comprehensive performance indicator called OBJ was proposed to synthesize the evaluation indicators:

$$\mathrm{OBJ} = \frac{1}{2}\left(\frac{\mathrm{SI_{tr}} + \mathrm{MAPE_{tr}}}{\mathrm{R^2_{tr}}}\right) + \frac{1}{2}\left(\frac{\mathrm{SI_{te}} + \mathrm{MAPE_{te}}}{\mathrm{R^2_{te}}}\right) \tag{11}$$

where the subscripts of tr and te represent the training set and the testing set, respectively. It should be noted that as the order of magnitude of RMSE is much higher than those of the other evaluation metrics, and meanwhile, SI and RMSE are closely correlated, this paper integrated R^2, SI, and MAPE to calculate the OBJ value. At the same time, the same weight (i.e., 1/2) was used for the model performance of the training set and testing set, considering that the two are equally important for evaluating the overall performance. By doing so, the integrated performance of a model can be ranked from the worst to the best according to the OBJ value. A lower OBJ value represents a better overall prediction performance.

5. Model development and discussion

5.1. Dimensionality reduction

Linear correlations between inputs and output can introduce the undesirable effect of information duplication. If they are ignored in developing ML models, wrong conclusions may be drawn. Therefore, it is important to perform collinearity diagnosis before ML modeling and reduce the dimensionality of inputs if necessary. In this study, a linear regression analysis was used to identify the collinearity for input variables.

Some evaluation indexes to quantify the extent of collinearity have been proposed, such as the pairwise correlation coefficient, the condition index, and the variance inflation factor (VIF) [61]. The VIF refers to the ratio of the variance between input variables with and without multicollinearity, which can reflect the degree of increase in variance caused by multicollinearity. VIF can be determined as follows:

$$VIF_i = 1/(1 - R_i^2) \tag{12}$$

where R_i represents the square of the multiple correlation coefficient between the i^{th} input variable and the rest. The closer the VIF value is to 1, the less collinearity it is, and vice versa. Generally, a VIF value greater than 10.0 is used as a collinearity indicator [62]. When VIF is less than 10.0, it can be considered that there is no significant multicollinearity.

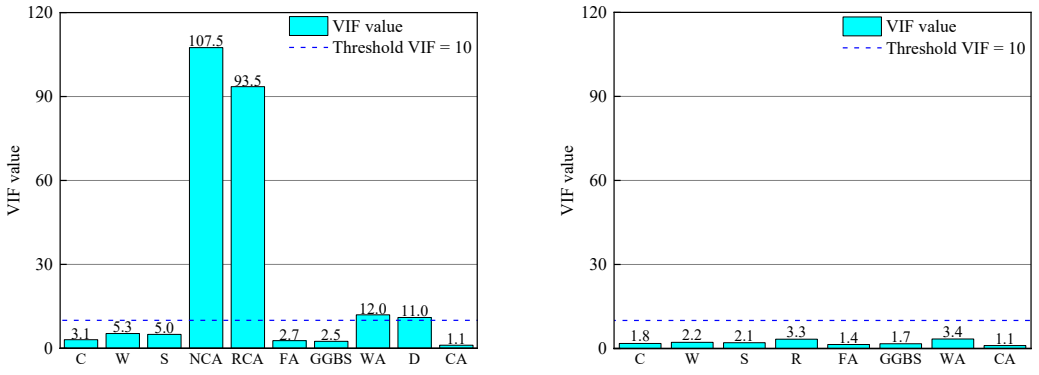

(a) Inputs without adjustment (b) Inputs after dimensionality reduction

Fig. 1. Results of the VIF value.

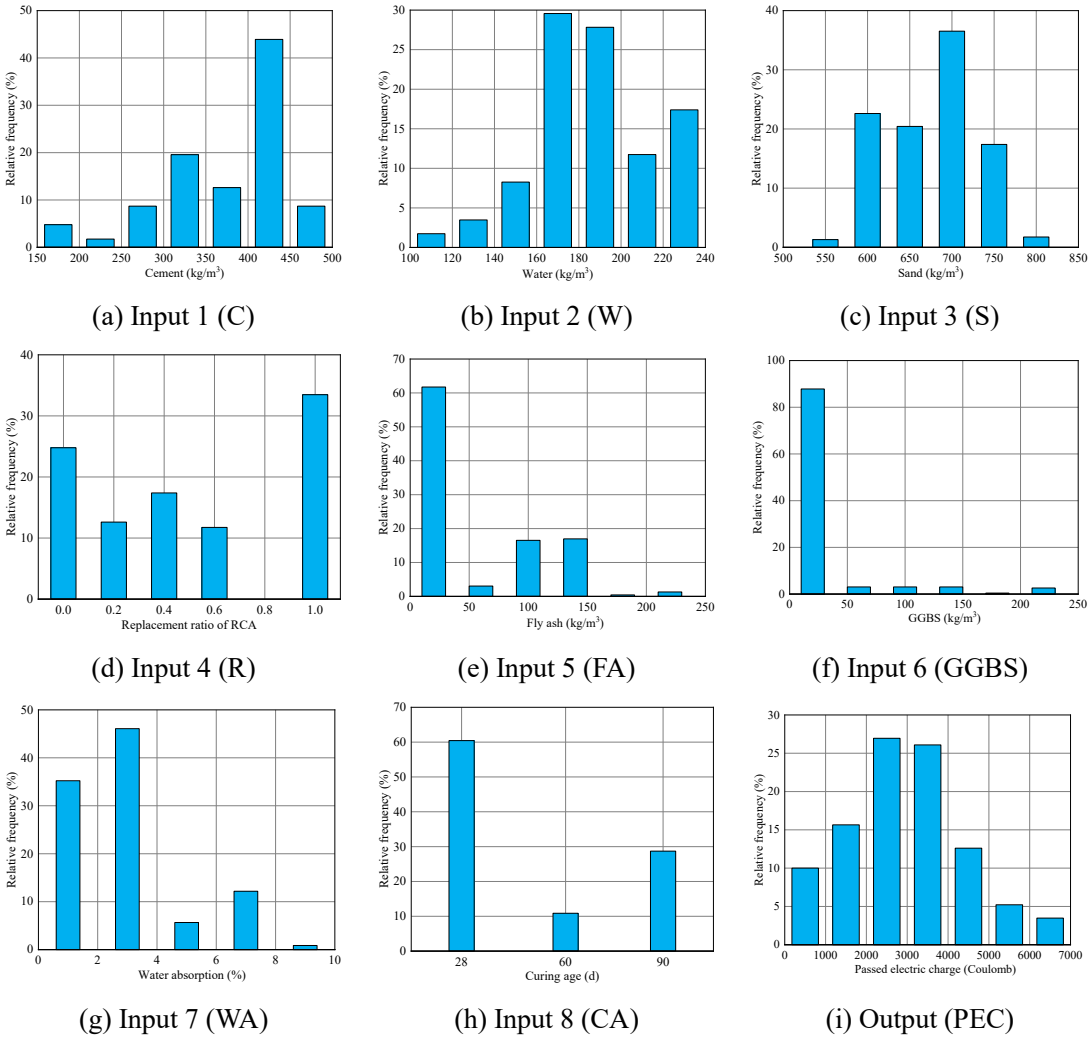

(a) Input 1 (C) (b) Input 2 (W) (c) Input 3 (S)

(d) Input 4 (R) (e) Input 5 (FA) (f) Input 6 (GGBS)

(g) Input 7 (WA) (h) Input 8 (CA) (i) Output (PEC)

Fig. 2. Frequency bar chart for each variable.

Fig. 1(a) shows the VIF values of the 10 input variables. The VIF values of NCA, RCA, WA, and D are all greater than the threshold (=10.0), especially for NCA (VIF = 107.5) and RCA (VIF = 93.5). For ordinary concrete, the amount of coarse aggregates in the mixture is basically stable, accounting for around 50% of the total concrete weight [63]. This is equivalent to setting up a potential link between NCA and RCA, making their VIF values dramatically high. As to WA (VIF = 12.0) and D (VIF = 11.0), they are higher than 10.0 because the two variables are distributed in a relatively narrow range, but are intimately related to the quality of mixed coarse aggregates. In most cases, RCA with lower water absorption has a higher density as the attached mortar is usually more compact.

Table 1
Statistical information for input and output variables (226 samples).

Attribute	C	W	S	R	FA	GGBS	WA	CA	Q *
Unit	kg/m^3	kg/m^3	kg/m^3	–	kg/m^3	kg/m^3	%	d	C
Maximum	485	225	780	1	225	214	9.6	90	6910
Minimum	176	117	530	0	0	0	0.5	28	444
Average	361	183	674	0.50	47	16	3.0	49	2985
Standard deviation	74	28	55	0.40	62	46	1.9	28	1444

Note: Q represents the passed electric charge (PEC) in Coulomb (C).

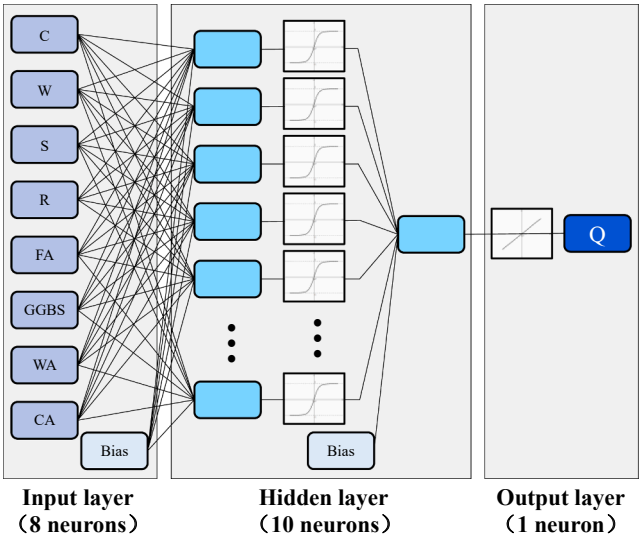

Fig. 3. The ANN model structure.

To eliminate the potential effect of collinearity, some adjustments were adopted. The variables NCA and RCA were combined into one variable, i.e., the replacement ratio (R), which can be calculated as:

$$R = m_{RCA}/(m_{NCA} + m_{RCA}) \quad (13)$$

Further, the variable D was removed whereas WA was retained, given a more representative distribution of WA than that of D in the database.

Results of the VIF values of inputs after the dimensionality reduction are shown in Fig. 1(b). All VIF values are less than 10.0, indicating no significant collinearity among the input variables.

Fig. 2 shows the frequency distribution of each variable after the dimensionality reduction. The statistics (i.e., the maximum, minimum, mean, and standard deviation) for all variables (also including the output) are listed in Table 1.

5.2. Construction and comparison of predictive models

After the dimensionality reduction, eight variables including C, W, S, R, FA, GGBS, WA, and CA were set as inputs, and Q was set as the output. The whole ML framework was developed based on the MATLAB platform [64]. The source codes can be obtained upon reasonable request.

5.2.1. Model development

The experimental dataset was randomly divided into the training set (80%) and the testing set (20%). For the ANN model implemented in the framework, the activation functions in the hidden layer and output layer were set as the hyperbolic tangent function and linear transfer function, respectively. The back-propagation algorithm was adopted to train the three-layer feedforward network [65,66]. The number of neurons for the hidden layer was a hyperparameter to be tuned. Fig. 3 shows the structure of the ANN model developed. For the GPR model, four kernel functions including the quadratic rational kernel, the Matern kernel, the exponential kernel, and the squared exponential kernel, were tested and compared with each other. For the SVR model, three kernel functions including the linear kernel, polynomial kernel, and Gaussian kernel were tested to determine the optimum one. For the CART model, the maximum tree depth and the minimum number of leaf node observations are two hyperparameters that need to be optimized and can also be used to prevent overfitting. For the RF model, two hyperparameters, the number of decision trees and the minimum leaf size, need to be

Table 2
The range and optimal value of hyperparameters for ML models.

Model type	Hyperparameters		
	Type	Range *	Optimal value
ANN	number of neurons in the hidden layer	[5:1:20]	10
GPR	kernel function	quadratic rational kernel, Matern kernel, exponential kernel, squared exponential kernel	squared exponential kernel
SVR	kernel function	linear kernel, polynomial kernel, Gaussian kernel	polynomial kernel with three order
CART	maximum tree depth	[4:1:10]	9
	minimum leaf size	[2:1:10]	2
RF	number of decision trees	[10:10:100]	50
	minimum leaf size	[2:1:10]	2
GBDT	number of decision trees	[10:10:100]	60
	minimum leaf size	[2:1:10]	2
	learning rate	[0.05,0.05,0.50]	0.10

* The values in brackets are the lower limit, step size, and upper limit for the range of each hyperparameter in turn.

Table 3
Results of performance metrics for ML models.

Model	Dataset	R^2	RMSE	SI	MAPE	OBJ
ANN	Training	0.952	308.329	0.103	0.103	0.274
	Testing	0.925	473.002	0.158	0.148	
	All	0.945	347.562	0.116	0.112	
GPR	Training	0.969	245.234	0.082	0.075	0.272
	Testing	0.903	519.266	0.174	0.170	
	All	0.951	319.435	0.107	0.094	
SVR	Training	0.962	268.370	0.090	0.081	0.288
	Testing	0.906	517.926	0.174	0.187	
	All	0.946	333.568	0.112	0.102	
CART	Training	0.904	427.475	0.143	0.145	0.389
	Testing	0.891	558.596	0.187	0.222	
	All	0.900	456.721	0.153	0.161	
RF	Training	0.957	320.708	0.107	0.117	0.336
	Testing	0.918	554.919	0.186	0.216	
	All	0.945	379.302	0.127	0.137	
GBDT	Training	0.982	194.258	0.065	0.067	0.199
	Testing	0.958	360.935	0.121	0.131	
	All	0.975	237.158	0.079	0.080	

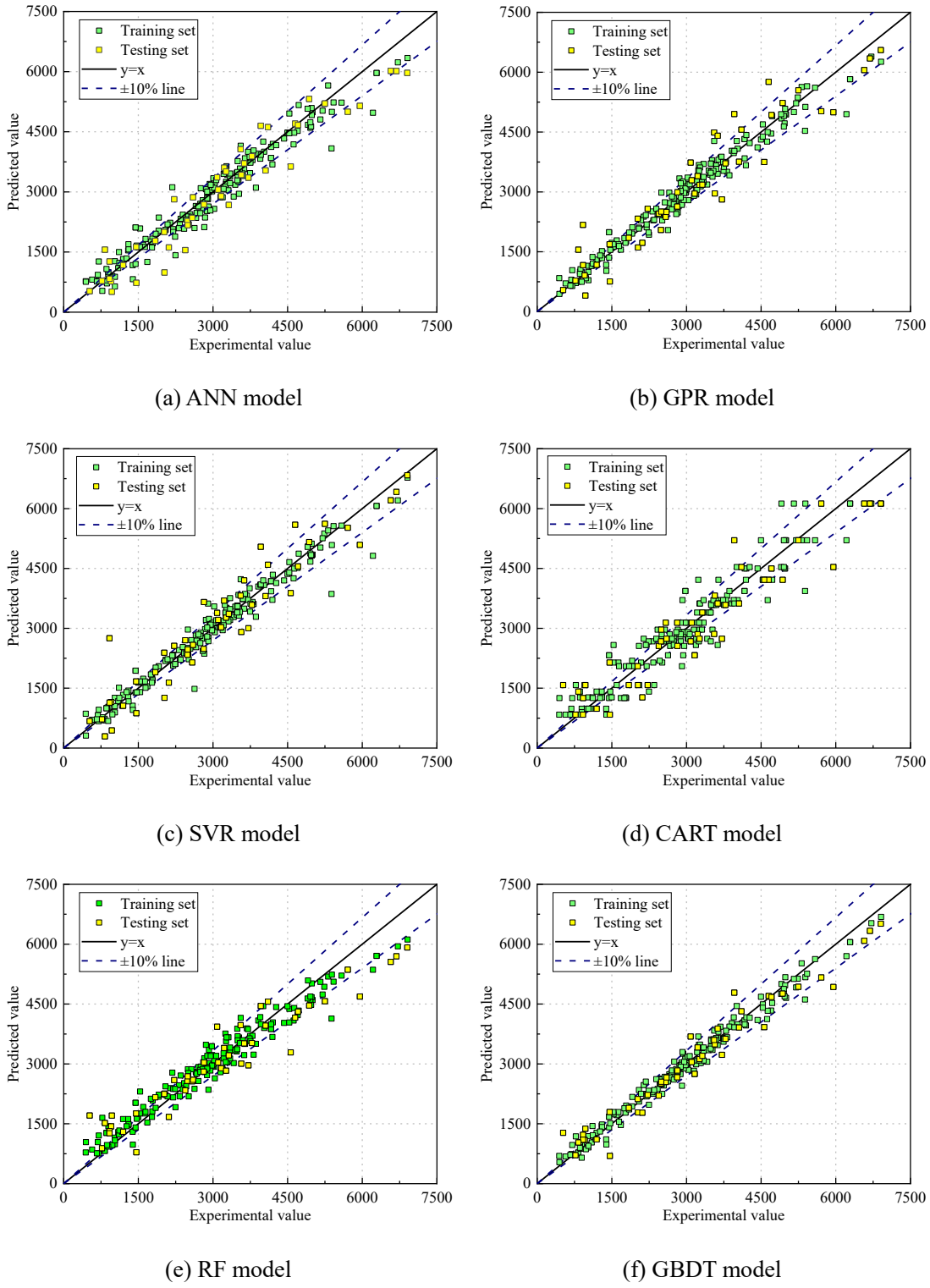

Fig. 4. Illustration of regression plot between the actual and predicted value of PEC.

optimized, while for the GBDT model, besides the above two hyperparameters, the learning rate was also considered.

Grid search, random search, and Bayesian optimization are three common hyperparameter optimization methods [67]. Considering the small number of hyperparameters involved in the ML models used in this study, the grid search in combination with 10-fold cross-validation was used to determine the hyperparameter values of each model. The range and optimal values for each hyperparameter are shown in Table 2. Other model parameters are set as default values.

5.2.2. *Model validation*

Table 3 summarizes the performance metrics of all the ML models integrated into the framework. Clearly, all the models show good performance in predicting the resistance to chloride penetration of RAC. Specifically, among the four standalone models, the GPR model has the best overall performance with the highest OBJ value of 0.272, slightly

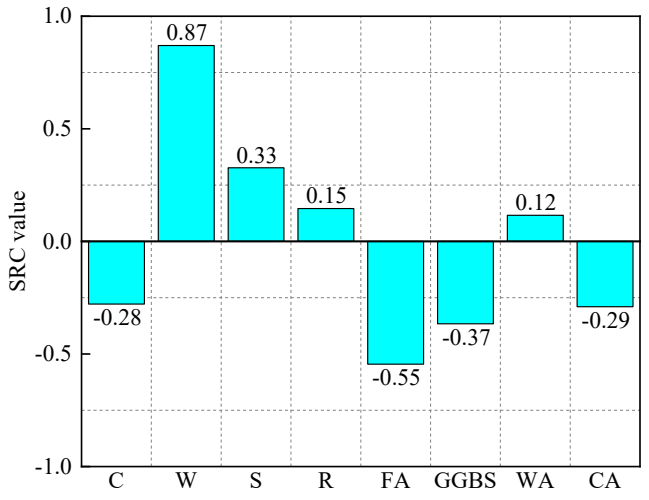

Fig. 5. The SRC value of input parameters.

surpassing the ANN model. Nevertheless, the GPR model performed well in the training set but shows a decreased accuracy in the testing sets. The GPR model can quantify the prediction uncertainty in a principled way, but the single kernel function limits its generalization ability to some extent. Meanwhile, the dataset used in this paper is not large (226 samples), so the adverse effect of the computational complexity of the GPR model is negligible. The ANN model, in contrast, achieved similar good performance in both sets, reflecting a better generalization ability. This may be due to the optimization of the structure of the neural network, i.e., the appropriate activation function and the number of neurons in the hidden layer after optimization. The performance of the SVR model is close to that of the ANN model, but the performance is decreased for test set. This is similar to the GPR model, limited by the kernel function. Compared with the other three standalone models, the CART model has the lowest R^2 value and the largest OBJ value, signaling a less accurate performance. The CART model is sensitive to data and prone to overfitting. Its generalization performance is generally improved by limiting the number of node samples and the depth of the tree, at the expense of the prediction accuracy.

When it comes to the two ensemble models, both the RF and GBDT yielded better results than the CART model, which proved the effectiveness of bagging and boosting algorithms, especially boosting algorithms. The GBDT model shows the best performance among all the ML models developed. Compared with the CART model, the relative improvement of the RF model and GBDT model is 5.0% and 8.3%, respectively, based on the R^2 value of the CART model. In addition, the GBDT model outperformed the RF model, as its OBJ value is reduced by approximately 40% relative to that of the RF model. The RF model can be highly parallelized to reduce the variance of the model, but its predictive performance is mediocre for data beyond the training set. The GBDT model integrates each weak learner based on the weight and has strong robustness to outliers, which makes it have better generalization ability.

To visualize the predictive performance, Fig. 4 shows the comparison between the experimental and predicted values. The better the model performance, the narrower the distribution area of data points. For each model, the data points are almost evenly distributed on both sides of the $y = x$ line, except for the RF model; it appears to underestimate the experimental values. Moreover, the data points for the CART model are the most scattered among all the models, being consistent with its maximum OBJ value (=0.389).

5.3. Model interpretability

Although the presently developed ML models have shown their good performance in predicting the chloride resistance of RAC, their interpretability is another critical issue. The more explainable the ML models, the more credible the prediction results, upon which more meaningful decisions can be made. The standardized regression coefficient (SRC) was utilized herein to identify the importance and impact of each input variable on the output. Then the robustness of the framework was verified by partial dependence analysis.

5.3.1. SRC analysis

As an instrumental index, SRC is determined by dividing a parameter estimate by the ratio of the sample standard deviation between input and output variables. After the data standardization, the influence of differences in dimension and order of magnitude is eliminated, so those different variables can be compared. SRC can therefore be used to compare the effects of different input variables on output variables. The SRC value ranges from −1 to 1. The greater the absolute value of SRC, the stronger the impact of input on output. A negative value represents the variable is inversely proportional to the output, while a positive one means the opposite is true.

Fig. 5 shows the SRC values computed for all the input variables. The water content has the highest absolute value of SRC (=0.87), more than 1.5 times the second place (FA content). This suggests the predominant role of water content (W) on the chloride penetration of RAC in terms of PEC. Then GGBS, C, S, and CA have statistically similar effects on PEC. In contrast, the RCA-related parameters, including R and WA, show relatively small effects on PEC, with their SRC values around 0.10. Moreover, the input variables W, S, R, and WA show positive effects on the output PEC, while C, FA, GGBS, and CA show the opposite. As a higher PEC value represents a lower chloride penetration resistance, the SRC values help identify the relative influence of each input. This mathematical information is indeed consistent with the physical behaviors observed in previous experiments. In specific, reducing the water-cement ratio (adding cement content and/or decreasing water content) [20], adding mineral admixtures [22–24], extending the curing time [21], and using high-quality aggregates [68] can help improve the resistance to chloride attack of RAC.

5.3.2. Partial dependence analysis

How each input affects output is a key real-world concern for model users. Partial dependence analysis not only provides a valuable pathway to uncover such information but also extracts design insights from the ML models. Partial dependence plots (PDPs) can visually display the dependency relationship between the target function and the features of interest. The influence of variations of the eight input variables on the chloride ion permeability of RAC was investigated by the two-way PDPs based on the best predictor, the GBDT model.

Fig. 6(a) to Fig. 6(e) disclose that as the curing age increases, a decreasing trend of passed electric charge can be observed, regardless of the changes in the amount of other materials (water, cement, sand, fly ash, and ground granulated blast slag). Surely, this trend corresponds to the fact that the chloride ion permeability becomes progressively weaker. Existing experiments [21] also demonstrate extending the curing age can increase the volume of hydration products and the compactness of RAC, which effectively slow down the chloride ion permeability.

The adverse effect of water content stands out when it exceeds 170 kg/m^3, while the beneficial effect of cement content is not obvious when it is lower than 420 kg/m^3 (Fig. 6(f)). This quantitative trend is intuitive as well as conducive to the durability design of RAC.

Changes in sand content will affect the void ratio and total surface area of aggregates in fresh concrete. At a given cement slurry, excessive sand (larger than 650 kg/m^3) will increase the total surface area and porosity of the aggregate, consume more cement to fill and wrap the aggregate, increase the porosity and adversely affect the permeability of RAC [69]. Interestingly, the threshold of 650 kg/m^3 is suggested in Fig. 6 (b).

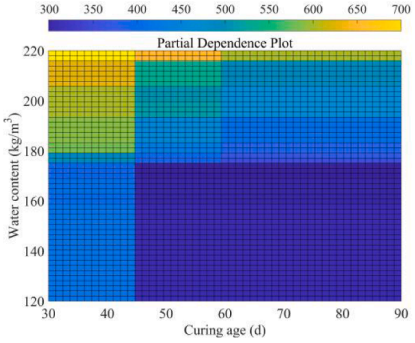

(a) Water content versus curing age

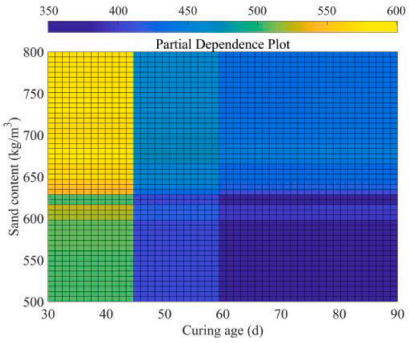

(b) Sand content versus curing age

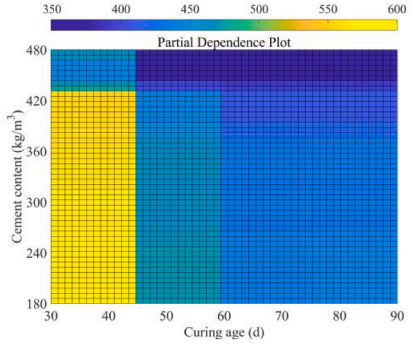

(c) Cement content versus curing age

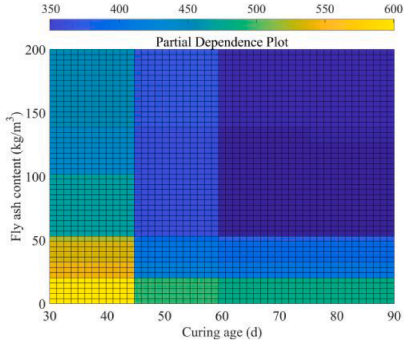

(d) Fly ash content versus curing age

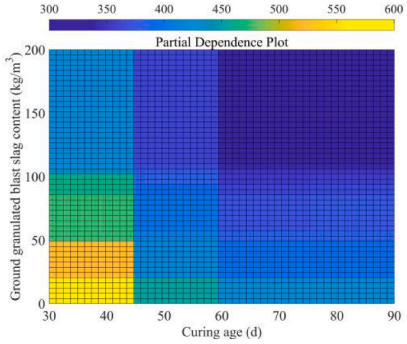

(e) GGBS content versus curing age

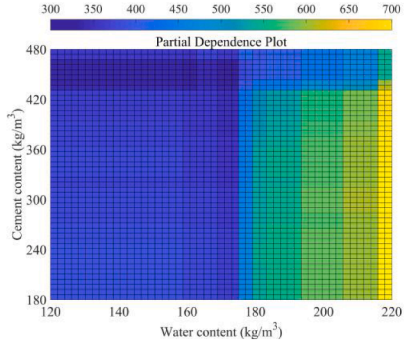

(f) Cement content versus water content

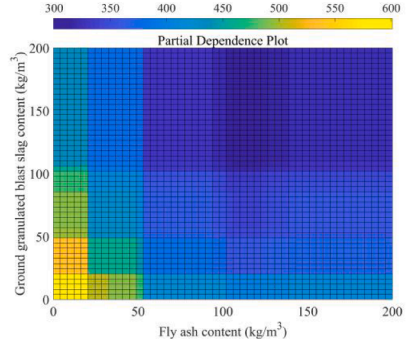

(g) GGBS content versus fly ash content

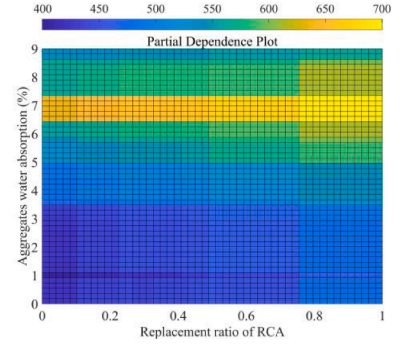

(h) Aggregates water absorption versus replacement ratio of RCA

Fig. 6. Two-way partial dependence plots for input variables.

Table 4
Chloride ion penetrability based on charge passed [71].

Charge passed (coulombs)	Chloride ion penetrability
>4000	High
2000~4000	Moderate
1000~2000	Low
100~1000	very low
<100	Negligible

Table 5
Requirements for passed electric charge (coulombs) of concrete [72].

Strength grade of concrete	Design working life		
	More than 100 years	More than 60 years	More than 30 years
<C30	<1500	<2000	<2500
C30~C45	<1200	<1500	<2000
≥C50	<1000	<1200	<1500

Fly ash and ground granulated blast slag can reduce the passed electric charge. Just adding more than 50 kg/m^3 of mineral admixtures (Fig. 6(d) and Fig. 6(e)) can effectively improve the chloride penetration resistance of RAC, even at a short curing age. As seen in Fig. 6(g), the combination use of fly ash and blast slag can also lead to improved chloride penetration resistance of RAC. Chloride ions exist in concrete mainly in three forms: chemical binding (in the form of Friedel's salt, $Ca_6Al_2O_6.CaCl_2{\cdot}10H_2O$), physical adsorption (adsorbed by calcium silicate hydrate (CSH) gel), and free state. The pozzolanic reaction of mineral admixtures can reduce the amount of cement hydration products $Ca(OH)_2$, improve the interface transition zone, and generate low-alkalinity CSH gel with higher strength and better stability [22,24]. This consequently lowers the porosity of cement paste, improves the pore structure of RAC, and then enhances the physical adsorption capacity of RAC. More low-alkalinity CSH gel increases the chemical combination of chloride ions.

Fig. 6(h) shows the PDP of the two parameters related to RCA. As the replacement rate of RCA increases, the passed electric charge tends to increase. It should be noted that the above trend is not obvious when the replacement rate is below 50%. When the water absorption of aggregates is lower than 7%, the increase in the water absorption is detrimental to the chloride penetration resistance of RAC. Nevertheless, the adverse impact of large water absorption suddenly decreases when it exceeds 7%. This may be explained as follows. The large water absorption of RCA is caused by the high porosity of the attached mortar. High porosity then increases the physical adsorption capacity of RAC to chloride ions to a certain extent, thereby improving its resistance to chloride ion erosion [29]. It should be noted that this limited positive effect is only effective against chloride ion erosion; the high porosity is detrimental when it comes to the mechanical performance of RAC.

6. Potential application of the proposed ML framework

6.1. Performance-based mixture design method

RAC mixture designs are mostly based on the traditional strength-based design method for NAC [70]. In this process, the durability of RAC is loosely guaranteed by additional restrictions, such as upper limits on water-cement ratio and lower limits on binder content. This durability design method has failed to keep up with modern design requirements, which raise higher expectations for precise control of durability and more sustainable constructions. Under this background, the establishment of a performance-based RAC mixture design method in conjunction with durability evaluation indicators is the key to improving RAC's service life reliability.

ASTM C1202 [71] classifies the chloride ion penetrability of concrete into five grades based on the passed electric charge (Table 4). Similarly, TB10005-2010 [72] puts forward requirements for the upper limit of the passed electric charge of concrete in terms of the design working life and the strength grade of concrete (Table 5).

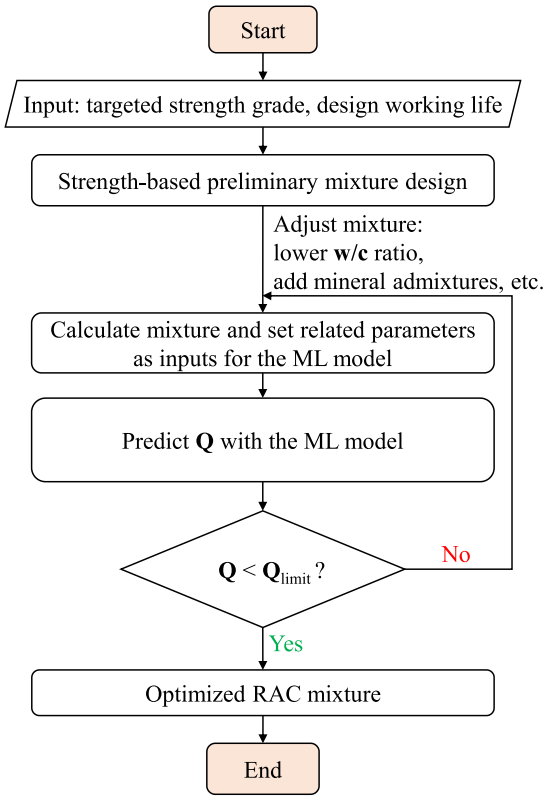

Fig. 7. The flow chart of performance-based mixture design method of RAC.

As illustrated above, the ML modeling framework proposed in this paper can accurately predict the passed electric charge of RAC. This superiority can be further harvested with the strength-based mixture design method to dynamically adjust the mixture parameters according to the prediction results, to optimize the dosage of each ingredient.

The specific implementation process is shown in Fig. 7. First, the targeted strength grade and design working life for RAC are set as inputs. The strength-based mixture design method is then used to determine the initial amount of each gradient, which is also the input for the ML models. Afterward, the passed electric charge values can be predicted and compared with the threshold value to verify the acceptability of the mixture, either by adjusting the controlling parameters (such as lowering water/cement (w/c) ratio, adding mineral admixtures, etc.) for re-verification or by outputting the optimized mixture according to the feedback.

6.2. Service life prediction model for RAC

Service life prediction models can be used to design, construct and maintain structures with expected service life, thereby reducing the life cycle cost [73]. In a chloride environment, the corrosion process of reinforced concrete structures can be divided into three stages, namely, the corrosion induction stage, the corrosion development stage, and the corrosion damage stage. The period of the first stage accounts for more than 70% of the service life of concrete structures [74]. It is usually regarded as the service life of a concrete structure, and the remaining two stages are deemed as the surplus of the design life. The first stage begins when the concrete structure is exposed to the corrosion environment until the chloride ion concentration at the depth of the concrete cover reaches the critical concentration for steel corrosion.

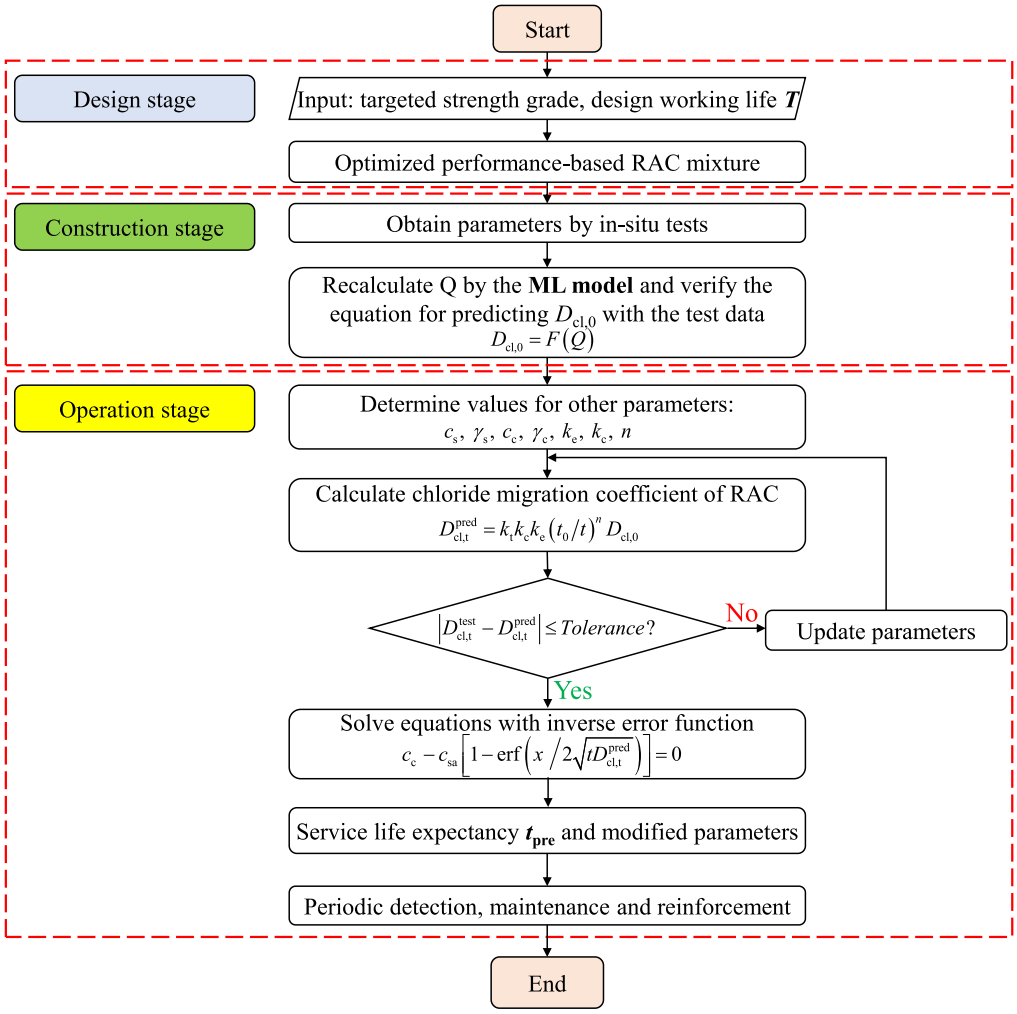

Fig. 8. The flow chart for establishing service life prediction model for RAC.

The existing service life prediction models of concrete structures in a chloride environment can be divided into three categories: original Fick's second law of diffusion, improved Fick's second law of diffusion, and physical models [75]. Among them, the improved Fick's second law is easy to use and can cover various exposure conditions. It is generally the first choice for the service life prediction of concrete structures. Representative methods are the DuraCrete method and Life-365 Computer program. The DuraCrete method is a design method based on probability reliability theory, which uses partial safety factor expressions for calculations. This paper developed a service life prediction model for RAC structures based on the DuraCrete method.

The model is carried out in three stages, as shown in Fig. 8. In the design stage, the preliminary mixture satisfying the requirements of strength grade and design working life T is given through the performance-based mixture design method described previously. In the construction phase, the material parameters and environmental condition parameters are determined through in-situ tests. There is a strong correlation between the passed electric charge and the chloride migration coefficient [74]. Inspired by that, a linear relationship between them for RAC was suggested by Silva et al. [76]:

$$D_{cl,0} = F(Q) = 0.0034Q \tag{14}$$

where $D_{cl,0}$ represents the chloride migration coefficient at age t_0, usually taken as t_0 for 28 days. Finally, in the operation stage, other model parameters including the surface chloride concentration c_s, partial safety factor γ_s, critical chloride concentration c_c, partial safety factor γ_c, environmental factor k_e, curing factor k_c, and age factor n, have not yet been available. The chloride ion diffusion coefficient of RAC at time t can be firstly calculated with default parameters. Based on in-situ test results, the model parameters are continuously revised and updated until the accuracy meets the requirements. Then the chloride ion diffusion coefficient is introduced into the analytical solution of Fick's second law to obtain the service life expectancy t_{pre} and output the revised model parameters. According to the expected service life, the RAC structure should be inspected regularly and performed maintenance and/or rehabilitation if necessary.

7. Conclusions

This paper explores how machine learning methods can be effectively leveraged for predicting the chloride penetration of RAC. The main conclusions are as follows:

(1) All the ML models incorporated into the framework show good performance in predicting the chloride resistance of RAC, with their R^2 values larger than 0.900. Among them, GBDT performs the best. With reference to the OBJ value, the overall performance of all the models can be ranked as GBDT > GPR > ANN > SVR > RF > CART;

(2) Based on the SRC analysis, the water content is identified as the most critical factor affecting the chloride ion permeability of RAC, followed by the content of FA and GGBS. Parameters related

Table A1
Experimental dataset.

Source	Sample ID
S.C. Kou et al. [50]	R0, R20, R50, R100, R0F25, R20F25, R50F25, R100F25, R0F35, R20F35, R50F35, R100F35.
S.C. Kou et al. [51]	R0, R20, R50, R100, R0F25, R20F25, R50F25, R100F25.
S.C. Kou et al. [52]	Control, C-FA35, C-GGBS55, RA50, RA50-FA35, RA50-GGBS55, RA100, RA100-FA35, RA100-GGBS55
M.H. Dai. [53]	A0, B0, B1, B2, C0, C1, C2.
C.S. Poon et al. [54]	R0, R50, R100, R0F25, R50F25, R100F25, R0F35, R50F35, R100F35, R0F55, R50F55, R100F55.
H. D. Zhen et al. [55]	NC30, C30RA1, C30RA2, C30RA3, NC45, C45RA1, C45RA2, C45RA3, NC60, C60RA1, C60RA2, C60RA3, NC80, C80RA1, C80RA2, C80RA3
Thomas et al. [56]	300/0.4/0, 300/0.4/0.25, 300/0.4/0.5, 300/0.4/1, 350/0.4/0, 350/0.4/0.25, 350/0.4/0.5, 350/0.4/1, 450/0.4/0, 450/0.4/0.25, 450/0.4/0.5, 450/0.4/1, 300/0.45/0, 300/0.45/0.25, 300/0.45/0.5, 300/0.45/1, 350/0.45/0, 350/0.45/0.25, 350/0.45/0.5, 350/0.45/1, 450/0.45/0, 450/0.45/0.25, 450/0.45/0.5, 450/0.45/1, 300/0.5/0, 300/0.5/0.25, 300/0.5/0.5, 300/0.5/1, 350/0.5/0, 350/0.5/0.25, 350/0.5/0.5, 350/0.5/1, 450/0.5/0, 450/0.5/0.25, 450/0.5/0.5, 450/0.5/1
Z. Pan et al. [57]	Control28, Control90
Bao et al. [58]	NC-0.33-0, NC-0.39-0, RC-II-0.33-30, RC-II-0.33-50, RC-II-0.33-100, RC-III-0.33-30, RC-III-0.33-50, RC-III-0.33-100, RC-III-0.39-30, RC-III-0.39-50, RC-III-0.39-100
W. S. Huai. [59]	Q0, Q35, Q50, Q0F10S20, Q0F15S15, Q0F20S10, Q35F10S20, Q35F15S15, Q35F20S10, Q50F15, Q50F30, Q50F50, Q50S15, Q50S30, Q50S50, Q50F10S20, Q50F15S15, Q50F20S10.
Duan et al. [60]	NC, RC1, RC2, RC3

to aggregates quality, such as water absorption and replacement ratio, have a less noticeable influence on the chloride permeability of RAC. As a trend, reducing water-cement ratio, adding mineral admixtures, extending curing time, and using high-quality aggregates have positive effects on the resistance of RAC to chloride penetration to varying degrees;

(3) The two-way PDPs visualize the influences of the input variables on the chloride ion permeability of RAC, which is consistent with previous experimental results. Consequently, the partial dependence analysis sheds light on better understanding the hidden mechanisms of the proposed ML models, clarifies its values in verifying the robustness of the ML models, and builds trust for potential model users;

(4) The application scenarios of the ML models are further extended. A performance-based RAC mixture design method and service life prediction model are established, which can be assembled into an intelligent decision-making system to help engineers improve design efficiency and, ultimately, reap further sustainability benefits from RAC applications.

The work presented in this paper falls under the category of data-driven predictive modelling, which is fundamentally fueled by the growing demand for sustainable concrete and constructions. All the models are trained using the database collected from laboratory experiments. Further research is therefore needed on the durability of RAC served in the natural environment.

Declarations of interest

None.

Data availability statement

The ML models supporting the findings of this study are available from the corresponding author by reasonable request.

CRediT authorship contribution statement

Kai-Hua Liu: Formal analysis, Writing – original draft, Project administration, Funding acquisition. **Jia-Kai Zheng:** Resources, Software. **Fernando Pacheco-Torgal:** Writing – review & editing. **Xin-Yu Zhao:** Data curation, Funding acquisition, Writing – review & editing, Supervision.

Declaration of Competing Interest

The authors declare that they have no known competing financial interests or personal relationships that could have appeared to influence the work reported in this paper.

Acknowledgments

This work was supported by the National Natural Science Foundation of China (52108123), Guangdong Basic and Applied Basic Research Foundation (2020A1515110101), and Guangdong Provincial Key Laboratory of Modern Civil Engineering Technology (2021B1212040003).

Appendix A

References

[1] A. Torres, J. Brandt, K. Lear, J. Liu, A looming tragedy of the sand commons, Science 357 (6355) (2017) 970–971, https://doi.org/10.1126/science.aao0503.
[2] C. Zhang, M. Hu, F.D. Maio, B. Sprecher, X. Yang, A. Tukker, An overview of the waste hierarchy framework for analyzing the circularity in construction and demolition waste management in Europe, Sci. Total Environ. 803 (2022), 149892, https://doi.org/10.1016/j.scitotenv.2021.149892.
[3] F. Pacheco-Torgal, Y. Ding, F. Colangelo, R. Tuladhar, A. Koutamanis, Advances in Construction and Demolition Waste Recycling: Management, Processing and Environmental Assessment, Woodhead Publishing, Oxford, 2020.
[4] V.W.Y. Tam, M. Soomro, A.C.J. Evangelista, A review of recycled aggregate in concrete applications (2000–2017), Constr. Build. Mater. 172 (2018) 272–292, https://doi.org/10.1016/j.conbuildmat.2018.03.240.
[5] K.P. Verian, W. Ashraf, Y. Cao, Properties of recycled concrete aggregate and their influence in new concrete production, Resour. Conserv. Recycl. 133 (2018) 30–49, https://doi.org/10.1016/j.resconrec.2018.02.005.
[6] T. Xie, A. Gholampour, T. Ozbakkaloglu, Toward the development of sustainable concretes with recycled concrete aggregates: comprehensive review of studies on mechanical properties, J. Mater. Civ. Eng. 30 (9) (2018) 04018211, https://doi.org/10.1061/(ASCE)MT.1943-5533.0002304.
[7] D. Pedro, J. de Brito, L. Evangelista, Durability performance of high-performance concrete made with recycled aggregates, fly ash and densified silica fume, Cem. Concr. Compos. 93 (2018) 63–74, https://doi.org/10.1016/j.cemconcomp.2018.07.002.
[8] S.M.S. Kazmi, M.J. Munir, Y. Wu, I. Patnaikuni, Y. Zhou, F. Xing, Influence of different treatment methods on the mechanical behavior of recycled aggregate concrete: a comparative study, Cem. Concr. Compos. 104 (2019), 103398, https://doi.org/10.1016/j.cemconcomp.2019.103398.
[9] K. Liu, C. Zou, J. Yan, Shear transfer behavior between substrate recycled aggregate concrete and new natural aggregate concrete, Struct. Concr. 22(2) (2021): 1022-1036. https://doi.org/10.1002/suco.201900570.
[10] A.M. Knaack, Y.C. Kurama, Sustained service load behavior of concrete beams with recycled concrete aggregates, ACI Struct. J. 112 (5) (2015) 565–577, https://doi.org/10.14359/51687799.
[11] J. Pacheco, J. de Brito, C. Chastre, L. Evangelista, Uncertainty models of reinforced concrete beams in bending: code comparison and recycled aggregate incorporation, J. Struct. Eng. 145 (4) (2019) 04019013, https://doi.org/10.1061/(ASCE)ST.1943-541X.0002296.
[12] K. Liu, J. Yan, M.S. Alam, C. Zou, Seismic fragility analysis of deteriorating recycled aggregate concrete bridge columns subjected to freeze-thaw cycles, Eng. Struct. 187 (2019) 1–15, https://doi.org/10.1016/j.engstruct.2019.01.134.
[13] M.U. Khan, S. Ahmad, H.J. Al-Gahtani, Chloride-induced corrosion of steel in concrete: an overview on chloride diffusion and prediction of corrosion initiation time, Int. J. Corros. 2017 (2017) 5819202, https://doi.org/10.1155/2017/5819202.
[14] H. Guo, C. Shi, X. Guan, J. Zhu, Y. Ding, T. Ling, H. Zhang, Y. Wang, Durability of recycled aggregate concrete–A review, Cem. Concr. Compos. 89 (2018) 251–259, https://doi.org/10.1016/j.cemconcomp.2018.03.008.
[15] C. Liang, Z. Cai, H. Wu, J. Xiao, Y. Zhang, Z. Ma, Chloride transport and induced steel corrosion in recycled aggregate concrete: a review, Constr. Build. Mater. 282 (2021), 122547, https://doi.org/10.1016/j.conbuildmat.2021.122547.

[16] M. Gomes, J. de Brito, Structural concrete with incorporation of coarse recycled concrete and ceramic aggregates: durability performance, Mater. Struct. 42 (5) (2009) 663–675, https://doi.org/10.1617/s11527-008-9411-9.
[17] S. Kou, C. Poon, Enhancing the durability properties of concrete prepared with coarse recycled aggregate, Constr. Build. Mater. 35 (2012) 69–76, https://doi.org/10.1016/j.conbuildmat.2012.02.032.
[18] C. Faella, C. Lima, E. Martinelli, M. Pepe, R. Realfonzo, Mechanical and durability performance of sustainable structural concretes: an experimental study, Cem. Concr. Compos. 71 (2016) 85–96, https://doi.org/10.1016/j.cemconcomp.2016.05.009.
[19] L. Evangelista, J. de Brito, Durability performance of concrete made with fine recycled concrete aggregates, Cem. Concr. Compos. 32 (1) (2010) 9–14, https://doi.org/10.1016/j.cemconcomp.2009.09.005.
[20] M. Tuyan, A. Mardani-Aghabaglou, K. Ramyar, Freeze-thaw resistance, mechanical and transport properties of self-consolidating concrete incorporating coarse recycled concrete aggregate, Mater. Des. 53 (2014) 983–991, https://doi.org/10.1016/j.matdes.2013.07.100.
[21] J. Sim, C. Park, Compressive strength and resistance to chloride ion penetration and carbonation of recycled aggregate concrete with varying amount of fly ash and fine recycled aggregate, Waste Manage. 31 (11) (2011) 2352–2360, https://doi.org/10.1016/j.wasman.2011.06.014.
[22] P. Saravanakumar, G. Dhinakaran, Durability aspects of HVFA-based recycled aggregate concrete, Mag. Concr. Res. 66 (4) (2014) 186–195, https://doi.org/10.1680/macr.13.00200.
[23] K. Kapoor, S.P. Singh, B. Singh, Durability of self-compacting concrete made with Recycled Concrete Aggregates and mineral admixtures, Constr. Build. Mater. 128 (2016) 67–76, https://doi.org/10.1016/j.conbuildmat.2016.10.026.
[24] J. Andal, M. Shehata, P. Zacarias, Properties of concrete containing recycled concrete aggregate of preserved quality, Constr. Build. Mater. 125 (2016) 842–855, https://doi.org/10.1016/j.conbuildmat.2016.08.110.
[25] N. Otsuki, S. Miyazato, W. Yodsudjai, Influence of recycled aggregate on interfacial transition zone, strength, chloride penetration and carbonation of concrete, ASCE J. Mater. Civ. Eng. 15 (5) (2003) 443–451, https://doi.org/10.1061/(ASCE)0899-1561(2003)15:5(443).
[26] Y.A. Villagrán-Zaccardi, C.J. Zega, Á.A. Di-Maio, Chloride penetration and binding in recycled concrete, ASCE J. Mater. Civ. Eng. 20 (6) (2008) 449–455, https://doi.org/10.1061/(ASCE)0899-1561(2008)20:6(449).
[27] M.C. Limbachiya, T. Leelawat, R.K. Dhir, Use of recycled concrete aggregate in high-strength concrete, Mater. Struct. 33 (9) (2000) 574–580, https://doi.org/10.1007/BF02480538.
[28] H. Mefteh, O. Kebaïli, H. Oucief, L. Berredjem, N. Arabi, Influence of moisture conditioning of recycled aggregates on the properties of fresh and hardened concrete, J. Cleaner Prod. 54 (2013) 282–288, https://doi.org/10.1016/j.jclepro.2013.05.009.
[29] C.J. Zega, L.R. Santillán, M.E. Sosa, Y.A. Villagrán Zaccardi, Durable performance of recycled aggregate concrete in aggressive environments, J. Mater. Civ. Eng. 32 (7) (2020) 03120002, https://doi.org/10.1061/(ASCE)MT.1943-5533.0003253.
[30] M.I. Jordan, T.M. Mitchell, Machine learning: trends, perspectives, and prospects, Science 349 (6245) (2015) 255–260, https://doi.org/10.1126/science.aaa8415.
[31] H. Salehi, R. Burgueño, Emerging artificial intelligence methods in structural engineering, Eng. Struct. 171 (2018) 170–189, https://doi.org/10.1016/j.engstruct.2018.05.084.
[32] S. Haykin, Neural Networks and Learning Machines, 3rd ed, Pearson Prentice Hall, New York, 2009.
[33] M. Mirrashid, H. Naderpour, Recent trends in prediction of concrete elements behavior using soft computing (2010–2020), Arch. Comput. Methods Eng. 28 (4) (2020) 3307–3327, https://doi.org/10.1007/s11831-020-09500-7.
[34] İ.B. Topçu, M. Sarıdemir, Prediction of mechanical properties of recycled aggregate concretes containing silica fume using artificial neural networks and fuzzy logic, Comput. Mater. Sci. 42 (1) (2008) 74–82, https://doi.org/10.1016/j.commatsci.2007.06.011.
[35] B.A. Omran, Q. Chen, R. Jin, Comparison of data mining techniques for predicting compressive strength of environmentally friendly concrete, J. Comput. Civ. Eng. 30 (6) (2016) 04016029, https://doi.org/10.1061/(ASCE)CP.1943-5487.0000596.
[36] Z. Duan, C.S. Poon, J. Xiao, Using artificial neural networks to assess the applicability of recycled aggregate classification by different specifications, Mater. Struct. 50 (2) (2017) 1–14, https://doi.org/10.1617/s11527-016-0972-8.
[37] E.M. Golafshani, A. Behnood, Application of soft computing methods for predicting the elastic modulus of recycled aggregate concrete, J. Cleaner Prod. 176 (2018) 1163–1176, https://doi.org/10.1016/j.jclepro.2017.11.186.
[38] H. Naderpour, A.H. Rafiean, P. Fakharian, Compressive strength prediction of environmentally friendly concrete using artificial neural networks, J. Build. Eng. 16 (2018) 213–219, https://doi.org/10.1016/j.jobe.2018.01.007.
[39] J. Xu, Y. Chen, T. Xie, X. Zhao, B. Xiong, Z. Chen, Prediction of triaxial behavior of recycled aggregate concrete using multivariable regression and artificial neural network techniques, Constr. Build. Mater. 226 (2019) 534–554, https://doi.org/10.1016/j.conbuildmat.2019.07.155.
[40] K. Liu, M.S. Alam, J. Zhu, J. Zheng, L. Chi, Prediction of carbonation depth for recycled aggregate concrete using ANN hybridized with swarm intelligence algorithms, Constr. Build. Mater. 301 (2021), 124382, https://doi.org/10.1016/j.conbuildmat.2021.124382.
[41] K. Liu, Z. Dai, R. Zhang, J. Zheng, J. Zhu, X. Yang, Prediction of the sulfate resistance for recycled aggregate concrete based on ensemble learning algorithms, Constr. Build. Mater. 317 (2022), 125917, https://doi.org/10.1016/j.conbuildmat.2021.125917.
[42] S. Lian, S. Ruan, S. Zhan, C. Unluer, T. Meng, K. Qian, Unlocking the role of pores in chloride permeability of recycled concrete: a multiscale and a statistical investigation, Cem. Concr. Compos. 125 (2022), 104320, https://doi.org/10.1016/j.cemconcomp.2021.104320.
[43] G. Yue, Z. Ma, M. Liu, C. Liang, G. Ba, Damage behavior of the multiple ITZs in recycled aggregate concrete subjected to aggressive ion environment, Constr. Build. Mater. 245 (2020), 118419, https://doi.org/10.1016/j.conbuildmat.2020.118419.
[44] D.E. Rumelhart, B. Widrow, M.A. Lehr, The basic ideas in neural networks, Commun. ACM 37 (3) (1994) 87–93.
[45] C.E. Rasmussen, Gaussian Processes in Machine Learning, Summer School on Machine Learning, Springer, Berlin, 2003.
[46] C. Cortes, V. Vapnik, Support-vector networks, Mach. Learn. 20 (3) (1995) 273–297.
[47] L. Breiman, J.H. Friedman, R.A. Olshen, C.J. Stone, Classification and Regression Trees, Routledge, London, 2017.
[48] J.H. Friedman, Greedy function approximation: a gradient boosting machine, Ann. Stat. 29 (5) (2001) 1189–1232. https://www.jstor.org/stable/2699986.
[49] X. Shi, N. Xie, K. Fortune, J. Gong, Durability of steel reinforced concrete in chloride environments: an overview, Constr. Build. Mater. 30 (2012) 125–138, https://doi.org/10.1016/j.conbuildmat.2011.12.038.
[50] S. Kou, C.S. Poon, Compressive strength, pore size distribution and chloride-ion penetration of recycled aggregate concrete incorporating class-F fly ash, J. Wuhan Univ. Technol.-Mat. Sci. Edit. 21 (4) (2006) 130–136, https://doi.org/10.1007/BF02841223.
[51] S. Kou, C.S. Poon, D. Chan, Influence of fly ash as a cement addition on the hardened properties of recycled aggregate concrete, Mater. Struct. 41 (7) (2008) 1191–1201, https://doi.org/10.1617/s11527-007-9317-y.
[52] S. Kou, C.S. Poon, F. Agrela, Comparisons of natural and recycled aggregate concretes prepared with the addition of different mineral admixtures, Cem. Concr. Compos. 33 (8) (2011) 788–795, https://doi.org/10.1016/j.cemconcomp.2011.05.009.
[53] M. Dai, Experimental Research on the Penetration Resistance of Chloride Ions of Recycled Aggregate Concrete, Fuzhou University, Fuzhou, China, 2013 in Chinese.
[54] S. Kou, C.S. Poon, Long-term mechanical and durability properties of recycled aggregate concrete prepared with the incorporation of fly ash, Cem. Concr. Compos. 37 (2013) 12–19, https://doi.org/10.1016/j.cemconcomp.2012.12.011.
[55] Z. Duan, C.S. Poon, Properties of recycled aggregate concrete made with recycled aggregates with different amounts of old adhered mortars, Mater. Des. 58 (2014) 19–29, https://doi.org/10.1016/j.matdes.2014.01.044.
[56] J. Thomas, N.N. Thaickavil, P.M. Wilson, Strength and durability of concrete containing recycled concrete aggregates, J. Build. Eng. 19 (2018) 349–365, https://doi.org/10.1016/j.jobe.2018.05.007.
[57] Z. Pan, J. Zhou, X. Jiang, Y. Xu, R. Jin, J. Ma, Y. Zhuang, Z. Diao, S. Zhang, Q. Si, W. Chen, Investigating the effects of steel slag powder on the properties of self-compacting concrete with recycled aggregates, Constr. Build. Mater. 200 (2019) 570–577, https://doi.org/10.1016/j.conbuildmat.2018.12.150.
[58] J. Bao, S. Li, P. Zhang, X. Ding, S. Xue, Y. Cui, T. Zhao, Influence of the incorporation of recycled coarse aggregate on water absorption and chloride penetration into concrete, Constr. Build. Mater. 239 (2020), 117845, https://doi.org/10.1016/j.conbuildmat.2019.117845.
[59] S. Wei, Research on Influence of Mineral Admixture on Chloride Corrosion Resistance and Frost Resistance of Recycled Concrete, China University of Mining and Technology, Xuzhou, China, 2020 in Chinese.
[60] Z. Duan, S. Jiang, J. Xiao, S. Hou, X. Chen, Effect of moisture condition of recycled coarse aggregate on the properties of concrete, J. Build. Mater. 24(3)(2021), 545-550. (in Chinese) https://doi.org/10.3969/j. issn.1007-9629.2021.03.014.
[61] C.F. Dormann, J. Elith, S. Bacher, C. Buchmann, G. Carl, G. Carré, J.R.G. Marquéz, B. Gruber, B. Lafourcade, P.J. Leitão, T. Münkemüller, C. McClean, P.E. Osborne, B. Reineking, B. Schröder, A.K. Skidmore, D. Zurell, S. Lautenbach, Collinearity: a review of methods to deal with it and a simulation study evaluating their performance, Ecography 36 (1) (2013) 27–46, https://doi.org/10.1111/j.1600-0587.2012.07348.x.
[62] G. James, D. Witten, T. Hastie, R. Tibshirani, An Introduction to Statistical Learning, Springer, New York, 2013.
[63] M.A. DeRousseau, J.R. Kasprzyk, W.V. Srubar III, Computational design optimization of concrete mixtures: a review, Cem. Concr. Res. 109 (2018) 42–53, https://doi.org/10.1016/j.cemconres.2018.04.007.
[64] MATLAB, Version 9.6.0 (R2019a), United States: The MathWorks, Inc., 2019.
[65] K. Levenberg, A method for the solution of certain non-linear problems in least squares, Q. Appl. Math. 2 (2) (1944) 164–168.
[66] D. Marquardt, An algorithm for least-squares estimation of nonlinear parameters, SIAM J. Appl. Math. 11 (1963) 431–441, https://doi.org/10.1137/0111030.
[67] R. Ghawi, J. Pfeffer, Efficient hyperparameter tuning with Grid Search for text categorization using kNN approach with BM25 similarity, Open Comput. Sci. 9 (1) (2019) 160–180, https://doi.org/10.1515/comp-2019-0011.
[68] D. Soares, J. de Brito, J. Ferreira, J. Pacheco, Use of coarse recycled aggregates from precast concrete rejects: mechanical and durability performance, Constr. Build. Mater. 71 (2014) 263–272, https://doi.org/10.1016/j.conbuildmat.2014.08.034.
[69] D. Bondar, S. Nanukuttan, J.L. Provis, M. Soutsos, Efficient mix design of alkali activated slag concretes based on packing fraction of ingredients and paste thickness, J. Cleaner Prod. 218 (2019) 438–449, https://doi.org/10.1016/j.jclepro.2019.01.332.

[70] C. Jiménez, M. Barra, A. Josa, S. Valls, LCA of recycled and conventional concretes designed using the Equivalent Mortar Volume and classic methods, Constr. Build. Mater. 84 (2015) 245–252, https://doi.org/10.1016/j.conbuildmat.2015.03.051.
[71] American Society for Testing and Materials–ASTM, ASTM-C1202: Standard test method for electrical indication of concrete's ability to resist chloride ion penetration, United States: West Conshohocken, 2012.
[72] China Academy of Railway Sciences, TB 10005–2010: Code for Durability Design on Concrete Structure of Railway, China Railway Press, China, 2011 in Chinese.
[73] H. Beushausen, R. Torrent, M.G. Alexander, Performance-based approaches for concrete durability: state of the art and future research needs, Cement Concrete Res. 119 (2019) 11–20, https://doi.org/10.1016/j.cemconres.2019.01.003.
[74] L. Yang, M. Zhou, Z. Chen, Quantitative analysis and design for durability of marine concrete structures, China Civ. Eng. J. 47(10)(2014), 70-79. (in Chinese) https://doi.org/10.15951/j.tmgcxb.2014.10.023.
[75] L. Tang, P. Utgenannt, D. Boubitsas, Durability and service life prediction of reinforced concrete structures, J. Chinese Ceram. Soc. 43 (10) (2015) 1408–1419, https://doi.org/10.14062/j.issn.0454-5648.2015.10.11.
[76] R.V. Silva, J.d. Brito, R. Neves, R. Dhir, Prediction of chloride ion penetration of recycled aggregate concrete, Mat. Res. 18 (2) (2015) 427–440, https://doi.org/10.1590/1516-1439.000214.